



Article

Tribological Properties of Hard TiB₂ Thin Films Prepared at Low Temperatures Using HiPIMS

Jianjian Yu ^{1,2,3}, Ping Zhang ^{1,2,3,*}, Puyou Ying ^{1,2,3} , Changhong Lin ^{1,2,3} , Tao Yang ^{1,2,3}, Jianbo Wu ^{1,2,3}, Chen Li ⁴, Min Huang ⁵ and Vladimir Levchenko ^{1,2,3,*}

¹ International Joint Institute of Advanced Coating Technology, Taizhou University, Taizhou 318000, China; yujianjian06@126.com (J.Y.); ypu@tztc.edu.cn (P.Y.); lin201191@163.com (C.L.); yangtaochd@163.com (T.Y.); wujb@tztc.edu.cn (J.W.)

² Wenling Research Institute, Taizhou University, Taizhou 318000, China

³ Zhejiang Provincial Key Laboratory for Cutting Tools, Taizhou University, Taizhou 318000, China

⁴ Science and Technology on Surface Engineering Laboratory, Lanzhou Institute of Physics, Lanzhou 730000, China; 13919169507@163.com

⁵ Civil Aviation Department, Zhejiang Institute of Communication, Hangzhou 311112, China; mhmater@163.com

* Correspondence: zhangp03@126.com (P.Z.); vladlev@yahoo.com (V.L.)

Abstract: Magnetron-sputtered WS₂ composite thin films are solid lubricants with excellent performances. However, the low hardness of the WS₂ thin films necessitates the further improvement of their wear resistance. For this purpose, an effective strategy is to alternately deposit or codeposit WS₂ and a hard phase, such as TiB₂, to form hard lubricant thin films. Herein, a TiB₂ thin film was prepared under the same conditions as those used for depositing the WS₂ thin film with a dense structure and excellent tribological properties. Because of the high deposition energy of high-power impulse magnetron sputtering (HiPIMS), the TiB₂ thin film possesses a dense structure and leather-like flat surface (hardness = 24.17 GPa). The friction coefficient of the film under different loads ranges between 0.6 and 0.8. The wear rate of the thin film increases with load, mainly because of fatigue wear and abrasive wear. Under high loads, obvious furrow-like wear marks are observed. At different sliding frequencies, except 8 Hz, the friction coefficient of the film ranges from 0.6 to 0.8. The main wear mode is fatigue wear, particularly at increasing sliding frequencies. Although the film possesses a relatively high friction coefficient, its wear resistance is excellent (minimum wear rate = $1.96 \times 10^{-6} \text{ mm}^3 / (\text{N}\cdot\text{m})$).

Keywords: TiB₂ thin film; tribological properties; hard thin film; low-temperature deposition; HiPIMS



Citation: Yu, J.; Zhang, P.; Ying, P.; Lin, C.; Yang, T.; Wu, J.; Li, C.; Huang, M.; Levchenko, V. Tribological Properties of Hard TiB₂ Thin Films Prepared at Low Temperatures Using HiPIMS. *Coatings* **2024**, *14*, 492. <https://doi.org/10.3390/coatings14040492>

Academic Editor: Stoyan Karakashev

Received: 19 March 2024

Revised: 8 April 2024

Accepted: 13 April 2024

Published: 16 April 2024



Copyright: © 2024 by the authors. Licensee MDPI, Basel, Switzerland. This article is an open access article distributed under the terms and conditions of the Creative Commons Attribution (CC BY) license (<https://creativecommons.org/licenses/by/4.0/>).

1. Introduction

Mutual friction and wear in mechanical equipment inevitably shorten the service life of its components and cause significant energy losses [1,2]. Therefore, studying the tribological properties of materials is crucial to reduce their surface friction coefficient and wear. Self-lubricating composite films are receiving increasing attention because of their excellent wear resistance and low coefficient of friction (COF) [3].

As transition metal sulfides with a layered structure, magnetron-sputtered WS₂ composite films are solid lubricant materials with satisfactory lubricating properties and stability [4]. However, pure WS₂ films possess poor wear resistance because of their loose structure and low hardness. Generally, the wear resistance of WS₂ films can be modified by doping with metal elements, such as Ti [5,6], Cr [7], Ni [8], and Al [9]. The addition of metal elements can effectively improve the hardness of WS₂-based composite films. Additionally, by increasing the deposition energy, the density and hardness of the WS₂ thin film can be increased, improving its wear resistance. Exploiting the high deposition energy of high-power impulse magnetron sputtering (HiPIMS), we prepared a pure WS₂

solid lubricating film possessing a dense structure and excellent wear resistance at a low temperature of 100 °C. The relevant results are awaiting publication separately. However, the film hardness is generally only 6–7 GPa and is suitable for application under low loads. Therefore, the wear resistance of the film under high loads requires further improvement.

To improve the hardness of WS₂-based composite films, an effective strategy is to alternately deposit or co-deposit WS₂ and a hard metal nitride phase, such as TiSiN [10], TiN [11,12], or TiAlSiN [13], to form hard lubricant thin films. However, the preparation of metal nitride hard coatings often requires high temperatures. TiB₂ exhibits substantially high hardness and satisfactory wear resistance [14–17] and is used for modifying WS₂ films [18,19]. Duan [18] et al. prepared a hard WS₂/TiB₂ self-lubricating composite thin film by co-sputtering a WS₂ target with a TiB₂ target to mix the soft phase of WS₂ with the hard phase of TiB₂. The results reveal that the thin film possesses a hardness of >20 GPa and a low COF (~0.2), and it demonstrates excellent antifriction and wear performances in wet environments. Liu [19] et al. demonstrated that compared with pure WS₂ films, the TiB₂-doped WS₂ composite thin films possess a dense amorphous structure with considerably improved oxidation resistance and mechanical properties. Moreover, hard-phase TiB₂ imparted thin films with excellent wear resistance and lubrication properties during friction at high temperatures [10]. Research has shown that the process parameters of magnetron sputtering (pulse, peak current, deposition temperature, deposition air pressure, etc.) have a certain influence on the properties of TiB₂ thin film [20]. Hellgren [21] et al. investigated that TiB₂ films deposited by HiPIMS on substrates at 500 °C always showed low B/Ti stoichiometry (titanium-rich), while the lack of stoichiometry could be reduced by regulating the increase of the pulse and peak current density.

A WS₂ solid lubricating film possessing a dense structure and excellent wear resistance was previously obtained at 100 °C using HiPIMS. Herein, a TiB₂ thin film was prepared under the same conditions as those used for depositing the WS₂ thin film. The microstructure, ingredient analysis, mechanical properties, and tribological properties of the deposited film were analyzed using scanning electron microscopy (SEM), X-ray Powder diffractometer (XRD), Nano-indentation and scratch testing, and tribometer. The results indicate that the TiB₂ thin film deposited at low temperatures exhibits a dense structure and high hardness. Although its friction coefficient is substantially high, the as-prepared film exhibits a satisfactory wear resistance.

2. Materials and Methods

2.1. Preparation of the Film

The TiB₂ thin film was prepared using HiPIMS technology by employing a pure Ti target (99.9% purity) and a TiB₂ target. The experimental instrument is an ion arc/magnetron sputtering composite coating machine (Beijing Powertech Technology Co., Ltd., Beijing, China; SP-0806ASI). Argon (99.9% purity) was used as the working gas. Polished stainless steel sheets (20 mm × 20 mm × 2 mm) and single-crystal silicon wafer sheets (100) were used as substrates. These substrates were separately cleaned in acetone (purity ≥ 99.5%; Zhejiang Hannuo Chemical Technology Co., Ltd., Taizhou, China) and anhydrous ethanol (purity ≥ 99.5%; Shanghai Chemical Reagent General Factory, Shanghai, China) for 20 min using an ultrasonic cleaner. Before deposition, the background vacuum was pumped to 5×10^{-3} Pa, and the chamber temperature was increased to 100 °C. Thereafter, argon was introduced in the chamber to achieve a pressure of 0.8 Pa.

Afterward, an ion source was employed to further clean the substrate surface with a bias voltage of 400 V. The glow plasma cleaning time was 30 min. Before depositing the TiB₂ thin film, a layer of the Ti film was pre-deposited to increase adhesion between the film and substrate. During Ti layer deposition, the power source voltage, current, pulse frequency, and pulse width of HiPIMS were 460 V, 25 A, 1000 Hz, and 100 μs, respectively. The substrate pulse bias, pulse width, and frequency were 50 V, 10 μs, and 75 kHz, respectively. The deposition time was 5 min. Subsequently, the TiB₂ layer was deposited. The power voltage, current, pulse frequency, and pulse width of HiPIMS during TiB₂ deposition were

580 V, 85 A, 1000 Hz, and 60 μ s, respectively. The substrate pulse bias, pulse width, and frequency were 60 V, 10 μ s, and 75 kHz, respectively. The deposition time was 60 min.

2.2. Structural, Compositional Characterization and Mechanical Properties of the Thin Film

SEM (Hitachi, Ltd., Tokyo, Japan, S-4800) was used to analyze the surface and cross-sectional morphologies of the TiB₂ thin film deposited on silicon wafers. The silicon wafer coated with a thin film was divided into two halves with tweezers, and then the cross-sectional morphology was observed under SEM. The crystal structure of TiB₂ was tested and analyzed by an X-ray diffractometer (Bruker Corporation, Bremen, Germany, D8 Advance), and the scanning speed was 5°/min, and the scanning range was 20°~85°. A NanoTest Vantage instrument (Micro Materials, Wrexham, UK, MML31CN) was employed to test the hardness (H) and elastic modulus (E) of the TiB₂ thin film. During testing, the indentation load was set to 15 mN. The indentation depth was ensured to be less than one-tenth of the thickness of the thin film. Sixteen points were measured on the sample, and the average value was calculated.

Experiments were conducted to characterize the bonding strength between the TiB₂ thin film and substrate using an automatic thin-film adhesion scratcher (Lanzhou Zhongke Kaihua Technology Development Co., Ltd., Lanzhou, China, WS-2005) and an optical microscope. Acoustic emission, dynamic load, and single reciprocation were adopted as the measurement method, operation mode, and reciprocation mode, respectively. The test load, loading rate, and scratch length were 40 N, 40 N/m, and 4 mm, respectively. Thereafter, optical microscopy was adopted to observe the scratch morphology to determine the critical loads of the three phases (L_{C1} and L_{C2}) [22,23].

2.3. Tribological Properties of the Thin Film

The tribological properties of the TiB₂ thin film were tested at room temperature using a multifunction tribometer (RTEC-Instruments Inc., Nanjing, China, MFT-5000) at different loads and sliding frequencies. A 6-mm-diameter SiC ball was employed as a frictional pair, and a linear reciprocating mode was adopted. The trace length and test time were 5 mm and 30 min, respectively.

COF can be obtained after the friction test using the software "MFT V22.3.28". The morphologies of the wear traces were obtained using an In-line Lambda 3D optical profilometer mounted on an MFT-5000 multifunction tribometer. The wear volume V can be obtained by using the software "MountainsMap Imaging Topography V9.2". The wear rate W was calculated using the following equation:

$$W = V / (F \times L), \quad (1)$$

where W is the wear rate ($\text{mm}^3/(\text{N}\cdot\text{m})$); V is the wear volume (mm^3); F is the applied load (N); and L is the total sliding length (m).

Additionally, to analyze the wear mechanism, SEM and energy dispersive spectrometry (EDS) were used to characterize the morphology and residual component of the wear traces. Figure 1 illustrates a flow chart for TiB₂ thin-film friction testing.

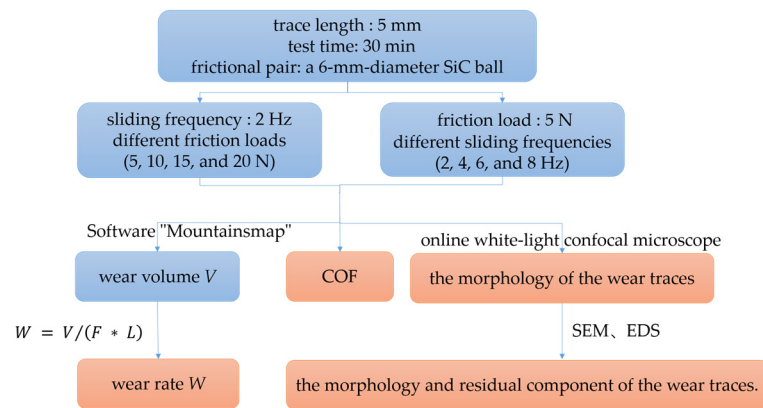


Figure 1. Flow chart of TiB₂ thin-film friction test process.

3. Results and Discussion

3.1. Morphological and Phase Analysis of the TiB₂ Thin Film

Figure 2a,b presents the surface topographies of the Ti transition layer and TiB₂ thin film deposited on a silicon substrate. As shown in the Figure, Ti thin film has a dense structure with very small and uniform grains. The TiB₂ thin film surface exhibits a dense structure and satisfactory surface quality with no obvious defects; however, the grain size is not uniform. Figure 3a,b depicts the cross-sectional topography of the TiB₂ thin film. The thin film exhibits layered deposition with a highly dense structure. HiPIMS has high deposition energy, so the deposited films always show layer growth and exhibit dense structures. The thicknesses of the TiB₂ thin film and transition Ti layer are ~1.4 and 0.4 μm, respectively.

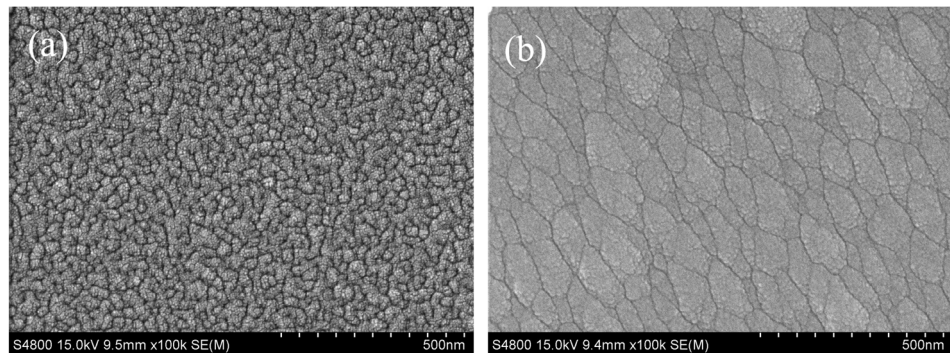


Figure 2. SEM images of the surface morphology of (a) the Ti transition layer and (b) the TiB₂ thin film at ×100 k.

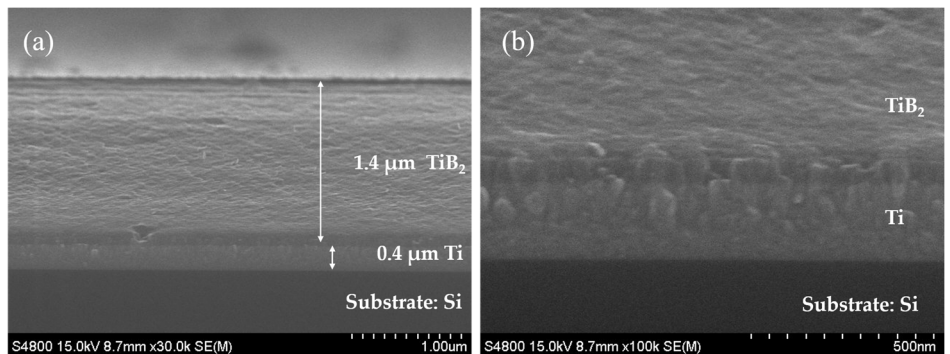


Figure 3. SEM images of the cross-sectional morphology of the TiB₂ thin film at (a) ×50 k and (b) ×100 k.

Figure 4 shows the XRD patterns of TiB₂ thin film prepared using HiPIMS. It can be seen that the deposited film exhibits a crystal phase near 27°. This crystal orientation often appears in TiB₂ thin films prepared using HiPIMS [21,24]. Meanwhile, strong diffraction peaks were also observed near 44°, corresponding to the (101) crystal phase of TiB₂. In addition, as shown in the Figure, many diffraction peaks with low intensity also appeared. From the XRD result, it can be seen that the prepared TiB₂ film is mainly composed of (001) and (101) crystal phases.

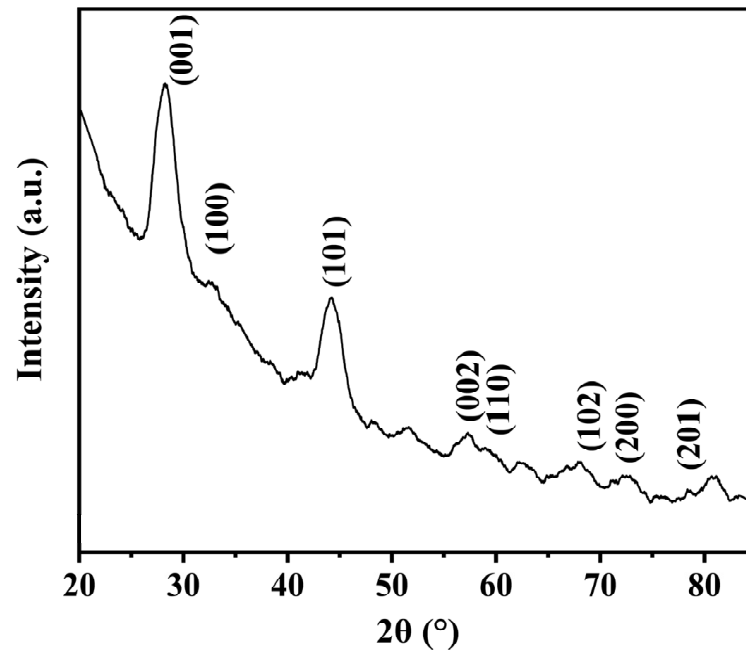


Figure 4. XRD patterns of deposited TiB₂ thin film.

3.2. Mechanical Properties of the TiB₂ Thin Film

The hardness (H) and approximate modulus of elasticity (E) of the TiB₂ thin film were obtained using the NanoTest Vantage system (Table 1). The deposited film possesses a high hardness of 24.17 GPa. The approximate modulus of elasticity was 256.80 GPa, and H/E and H^3/E^2 values were calculated as 0.0941 and 0.2141, respectively. The results indicate that the deposited film exhibits a satisfactory ability to resist crack formation and propagation [25]. These findings imply that TiB₂ thin films with high hardness and satisfactory mechanical properties can be prepared via HiPIMS at low temperatures.

Table 1. Hardness and approximate modulus of elasticity of the TiB₂ thin film.

Sample	H (GPa)	E (GPa)	H/E	H^3/E^2
TiB ₂	24.17	256.80	0.0941	0.2141

3.3. Analysis of the Bonding Force between the TiB₂ Thin Film and Substrate

Figure 5 depicts the acoustic emission spectrum obtained during the scratch test of the TiB₂ thin film. The acoustic emission peaks begin to appear at loads of approximately 13 and 17 N. However, the peaks at 13 and 17 N are substantially low, and the number of surrounding peaks is small. When the load exceeds 19.8 N, dense and high peaks begin to appear.

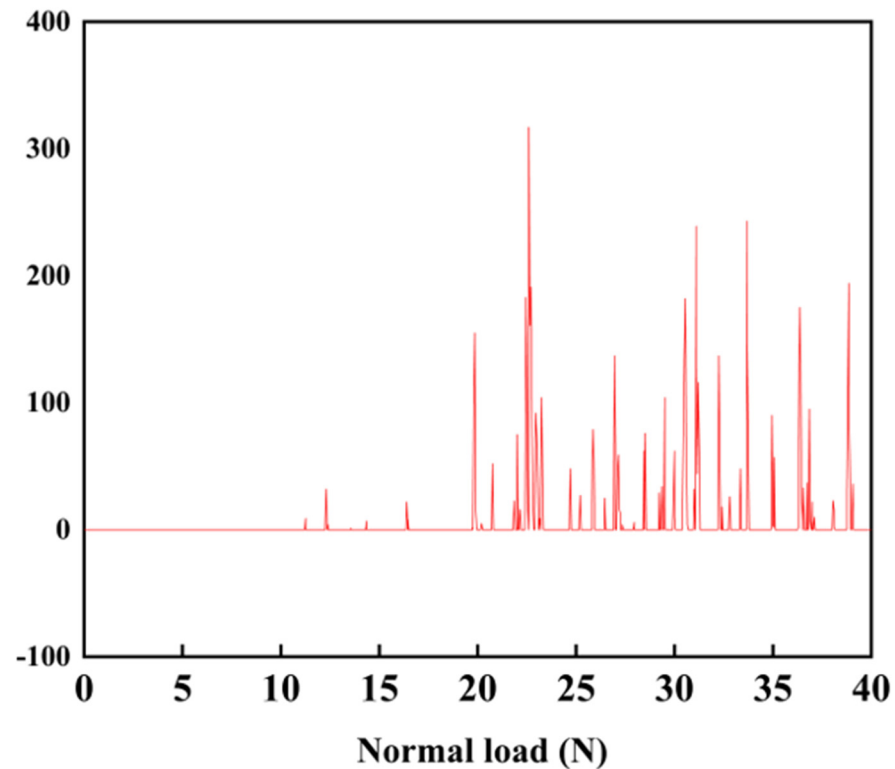


Figure 5. Acoustic emission folding diagram of the TiB₂ thin film.

Figure 6 presents the scratch morphology and a partially enlarged view of the scratch morphology obtained using an optical microscope. The three stages (I, II, and III) of coating failure and the values of critical loads (L_{C1} and L_{C2}) are clearly marked in the Figure. In stage I, the scratch is shallow, and only slight plastic deformation is present. In stage II, cracks appear in the scratch, and micro-cracks emerge on the surface of the film around the scratch. As the loading force increases, the scratch enters stage III, and more cracks form on the scratch. Simultaneously, long cracks appear on the surface of the film around the scratch, which is accompanied by the peeling off the film. Initially, some cracks were exhibited in stage II, and as the loading force increased, conformal cracking appeared in stage III. As the scratch load increases, buckling spallation initiates and intensifies [26,27]. When the loading force reaches near L_{C1} , a long crack is observed on the thin-film surface, and a piece of the thin film peels off in stage I. The crack formation and the peeling of the surface layer of the film led to the appearance of sporadic peaks at approximately 13 and 17 N in the acoustic emission spectrum. However, the interior of the scratch remains flat, so the loading force has not yet reached the critical load at this point.

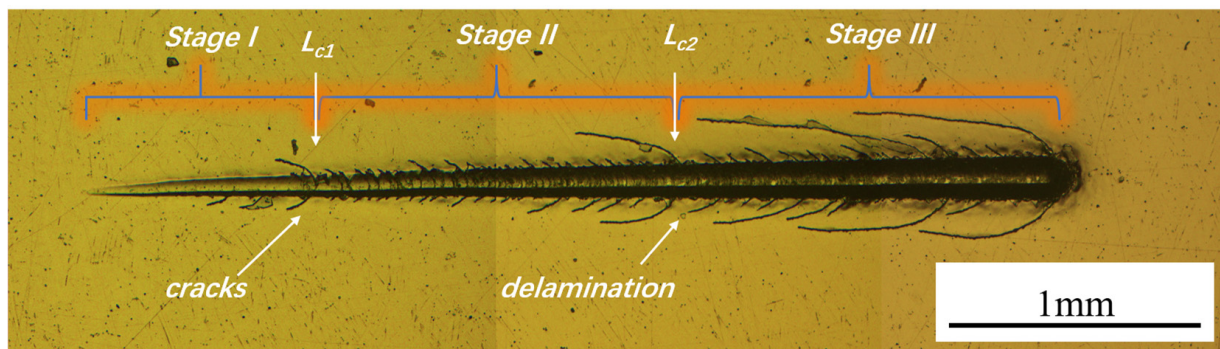


Figure 6. Optical map of a scratch of the TiB₂ thin film.

Based on Figures 5 and 6, the critical load of the thin film, L_C , can be concluded to be 19.8 N [28,29].

3.4. Tribological Properties of the TiB₂ Thin Film

3.4.1. Tribological Properties of the TiB₂ Thin Film under Different Loads

The tribological properties of the TiB₂ thin film under different friction loads (5, 10, 15, and 20 N) were tested using a tribometer in the linear reciprocating mode. Figure 7 depicts the friction coefficient of the TiB₂ thin film under different loads. Initially, significant fluctuations are observed in the friction coefficient, corresponding to the running stage of frictional wear. In the stable wear stage, the wear is slight, and the wear rate is stable. Overall, the friction coefficient of the thin film under different friction loads is approximately equivalent to 0.8. As a hard phase, the hardness of the TiB₂ particles is very large. So, the particles are not easy to be smoothed out during the friction process and cause a large frictional resistance. Resulting in a high COF with zigzagging unevenness. When the load is 5 N, the friction coefficient decreases to ~0.6 after ~700 s. When the load is 10 N, the friction coefficient gradually increases from approximately 0.7. The friction coefficient is more stable under the loads of 15 and 20 N.

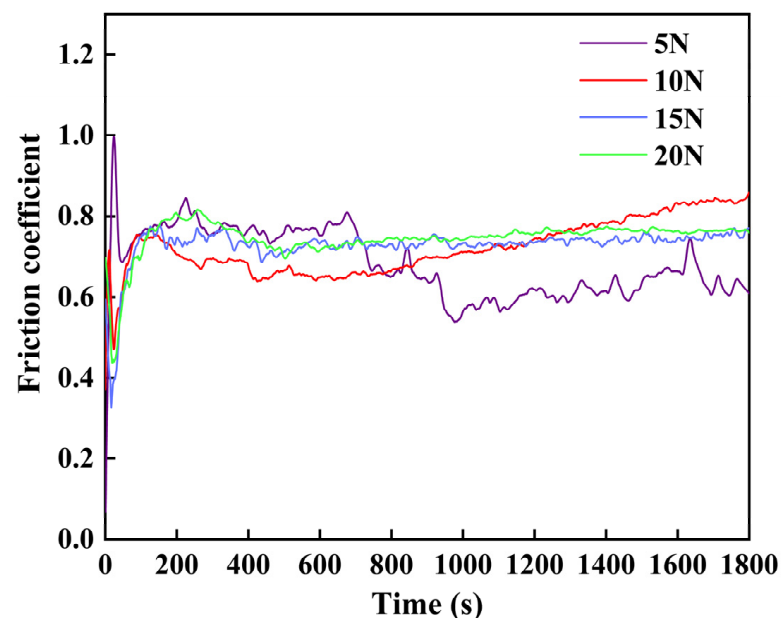


Figure 7. Friction coefficient of the TiB₂ thin film under different friction loads.

Table 2 and Figure 8 present the wear rates of the TiB₂ thin film under different loads at a sliding frequency of 2 Hz. The wear volume and wear rate correspondingly increase with an increase in the friction load. At a load of 5 N, the minimum wear rate is $3.66 \times 10^{-6} \text{ mm}^3/(\text{N}\cdot\text{m})$. The increase in the wear and wear rate may be related to the wear through the TiB₂ thin film.

Table 2. Wear rate of the TiB₂ thin film under different loads at a sliding frequency of 2 Hz.

Friction Load (N)	Total Sliding Length (m)	Wear Volume (μm^3)	Wear Rate ($10^{-6} \text{ mm}^3/(\text{N}\cdot\text{m})$)
5	36	658,448	3.66
10	36	4,089,657	11.36
15	36	7,263,526	13.45
20	36	11,716,428	16.27

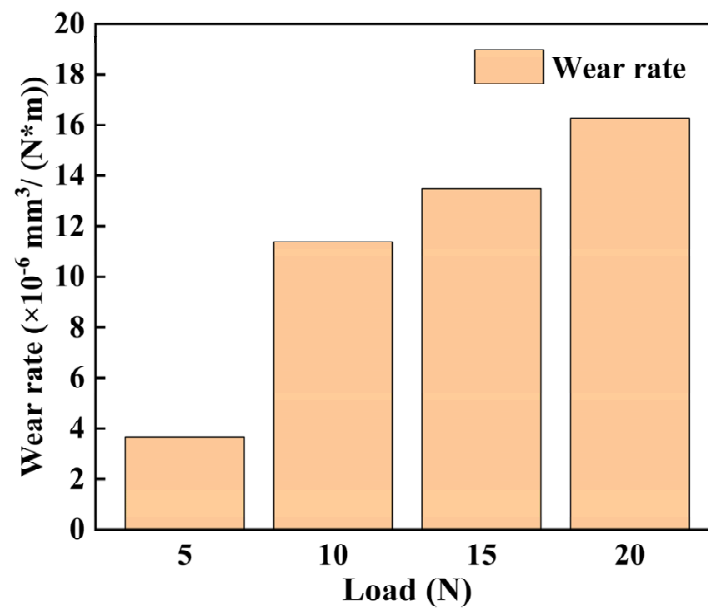


Figure 8. Histogram of the wear rate of the TiB_2 thin film under different loads.

Figure 9 presents the morphology of the wear traces on the surface of the TiB_2 thin film under different loads. At a load of 5 N, the wear trace was without any obvious defects except for two cracks. When the load is increased to 10 N, the wear marks become pronounced, and several micro-cracks appear. With increasing load, wear becomes more severe. Compared to the case under a load of 5 N, when the load is 20 N, the width of the wear scar increases by approximately two times, and the coating falls off, which is clearly observed using an optical microscope.

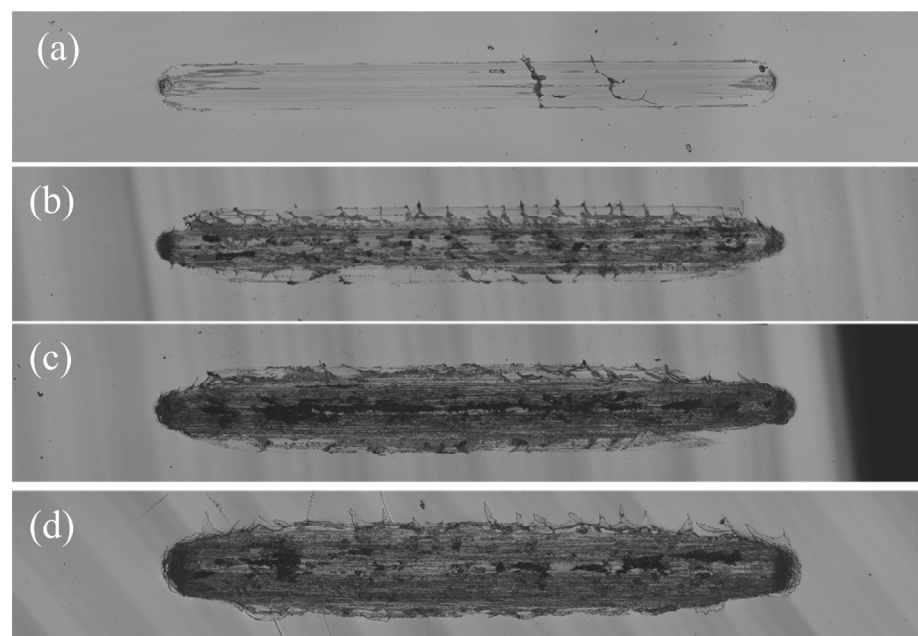


Figure 9. Morphological images of abrasion marks on the TiB_2 thin film under the friction loads of (a) 5, (b) 10, (c) 15, and (d) 20 N.

Figure 10 depicts the SEM images and EDS surface scanning analysis results of the local wear traces under different loads. Under a load of 5 N, a large amount of Ti remains on the surface of the wear trace. However, except in the crack, Fe was not detected. These results

imply that the coating has not been worn thoroughly. When the load increases to 10, 15, and 20 N, the amount of Ti on the worn surface decreases, whereas the Fe content increases. These findings are consistent with the characterization results of the worn cross-section.

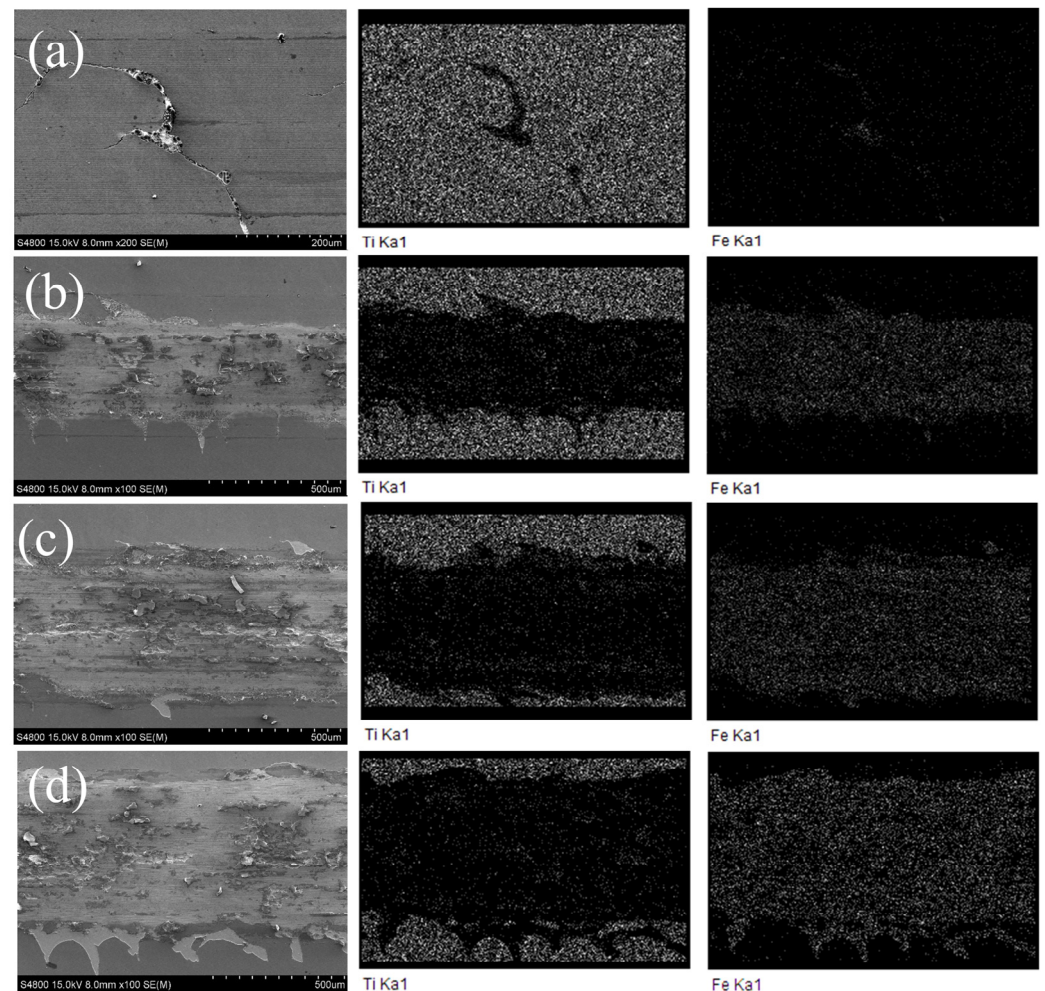


Figure 10. SEM images and EDS surface scanning analysis results of local wear traces under the loads of (a) 5, (b) 10, (c) 15, and (d) 20 N.

From the SEM images in Figure 10, with an increase in load, a significant increase in detachment is observed around the edge of the wear trace, and the detachment area increases. Based on the EDS results, TiB_2 and Ti layers have peeled off together. This indicates that the wear failure of the thin film may be related to the poor adhesion of the Ti layer to the substrate. Figure 11 depicts a local magnification of the TiB_2 thin-film abrasion at $500\times$ obtained using SEM. Figure 11a demonstrates a structure in which the plow-shaped grooves produced by abrasive wear are present in the wear marks. Granular-like debris repeatedly scratches the surface during friction, leaving abrasion marks on the surface [30]. Figure 11d presents a local magnification of the edge of the wear traces with obvious peeling off the thin film, with the Ti layer and TiB_2 thin film depicted in white and gray, respectively.

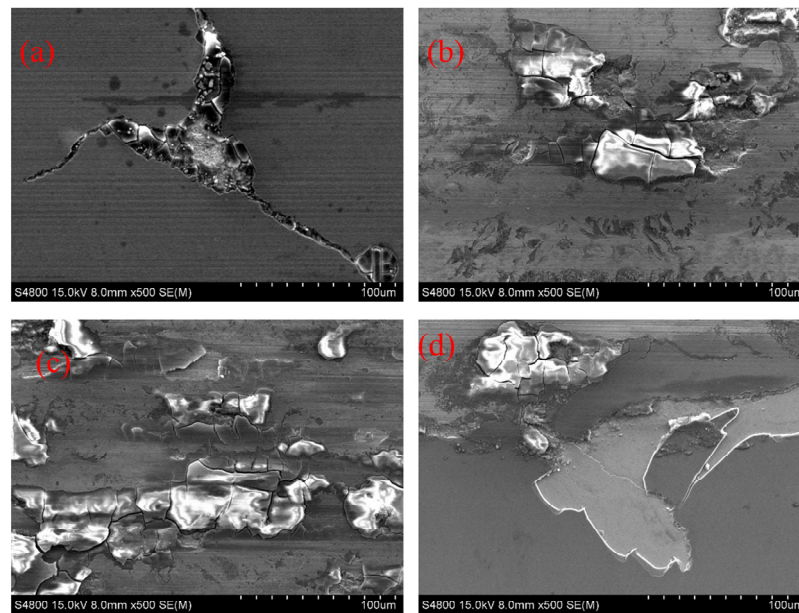


Figure 11. Local magnification of the abrasion marks on the TiB_2 thin film under the friction loads of (a) 5, (b) 10, (c) 15, and (d) 20 N.

3.4.2. Tribological Properties of the TiB_2 Thin Film at Different Sliding Frequencies

The tribological properties of the TiB_2 thin film at different sliding frequencies (2, 4, 6, and 8 Hz) were studied. Figure 12 illustrates the friction coefficient of the TiB_2 thin film at different sliding frequencies. At the beginning of the test, the friction coefficient fluctuated significantly. As mentioned earlier, at a sliding frequency of 2 Hz and a load of 5 N, the friction coefficient tends to be 0.6 after approximately 700 s. When the sliding frequency is 4 Hz, the friction coefficient fluctuates up and down at 0.7 throughout the experiment. At a sliding frequency of 6 Hz, the friction coefficient fluctuated at approximately 0.7 in the initial 400 s and subsequently stabilized at ~ 0.7 . At a sliding frequency of 8 Hz, the friction coefficient first gradually increased and then stabilized at ~ 0.95 after 400 s. This may be because of the falling of the debris shed by the thin film inside the scratch during the friction experiment, which increases the frictional resistance and consequently causes the final measured friction coefficient to be high.

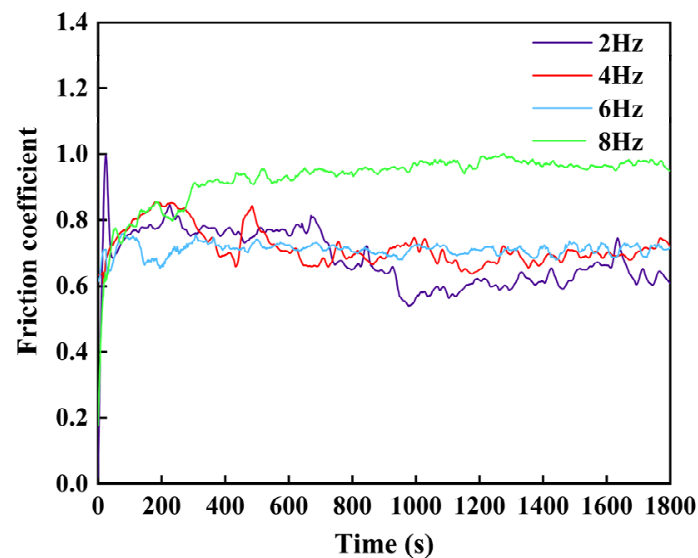


Figure 12. Friction coefficient of the TiB_2 thin film at different sliding frequencies.

Table 3 and Figure 13 present the wear rates of the TiB₂ thin film at different sliding frequencies under a load of 5 N. As the sliding frequency increases, the sliding length increases, and the volume of the wear trace also increases accordingly. According to the results, a wear rate of $1.96 \times 10^{-6} \text{ mm}^3/(\text{N}\cdot\text{m})$ was obtained at the sliding frequency of 4 Hz. However, under different sliding frequencies, the wear rate does not differ significantly, all within a small coefficient of $10^{-6} \text{ mm}^3/(\text{N}\cdot\text{m})$ level.

Table 3. Wear rate of the TiB₂ thin film at different sliding frequencies under a load of 5 N.

Sliding Frequency (Hz)	Total Sliding Length (m)	Wear Volume (μm^3)	Wear Rate ($\times 10^{-6} \text{ mm}^3/(\text{N}\cdot\text{m})$)
2	36	658,448	3.66
4	72	706,489	1.96
6	108	1,994,995	3.69
8	144	2,895,787	4.02

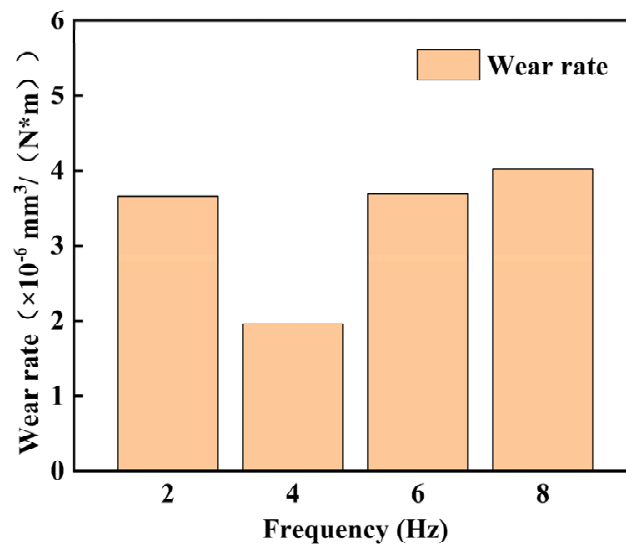


Figure 13. Histogram of the wear rate of the TiB₂ thin film at different sliding frequencies.

Figure 14 depicts the wear morphology of the TiB₂ thin film at the sliding frequencies of 2, 4, 6, and 8 Hz. The wear is least severe at the sliding frequency of 2 Hz. At the sliding frequency of 4 Hz, the wear is more severe, and certain fragmentations are observed at the center of the wear trace. This indicates that the thin film is about to wear out. At the sliding frequencies of 6 and 8 Hz, numerous dark areas appear in the images depicting the abrasion morphology. Subsequent SEM observations have confirmed that the thin film in these areas is worn through. As the sliding frequency increases, the wear becomes more severe, accompanied by the appearance of several cracks. Furthermore, the thin-film peeling phenomenon is observed.

Figure 15 presents the SEM images and EDS surface scanning analysis results of the local wear traces at different sliding frequencies. At the sliding frequency of 2 Hz, negligible wear-through was observed inside the abrasion marks. Moreover, the Fe element was observed in the crack. However, the Fe element was not detected elsewhere in the abrasion marks. This indicates that the film has not worn through. As the sliding frequency increases, the content of the Ti element progressively decreases in the middle of the wear marks, whereas that of the Fe element correspondingly increases.

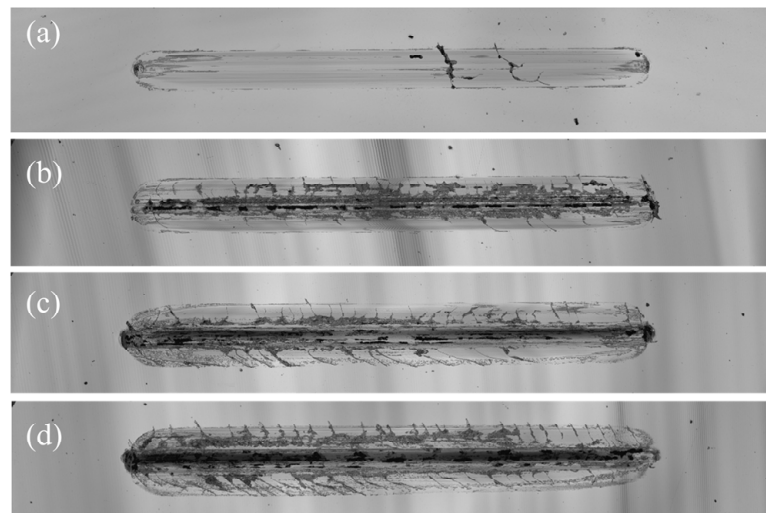


Figure 14. Wear morphology of the TiB₂ thin film at the sliding frequencies of (a) 2, (b) 4, (c) 6, and (d) 8 Hz.

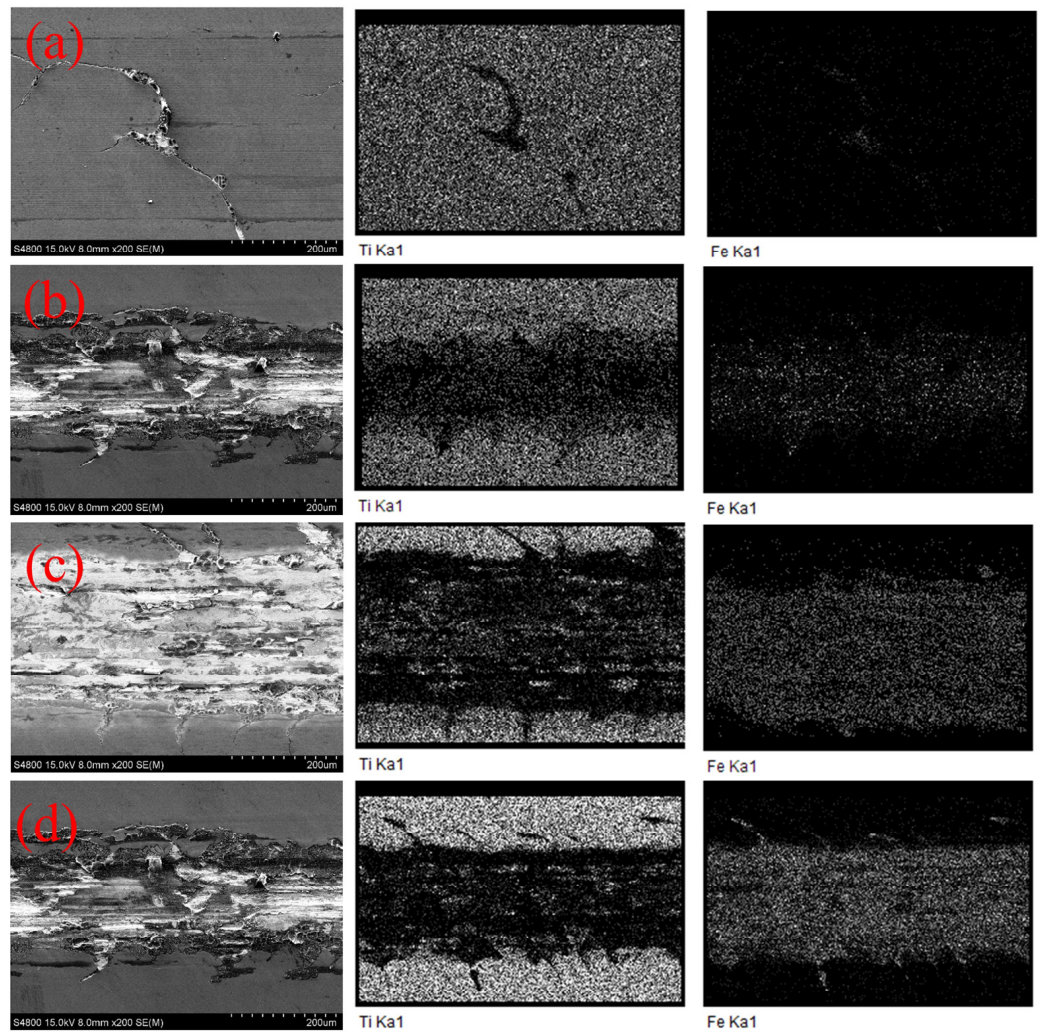


Figure 15. EDS patterns of TiB₂-coated abrasion marks at the sliding frequencies of (a) 2, (b) 4, (c) 6, and (d) 8 Hz.

Figure 16 presents a partial enlargement of the abrasion marks on the TiB₂ thin film at different sliding frequencies. Figure 16b–d depicts grooves formed by obvious plow wrinkles, which are typical of abrasive wear [31,32]. Herein, the plowing effect of abrasive wear causes damage to the trace surfaces, resulting in the wearing down of the film to the stainless steel substrate. Furthermore, pockmarks and cavities caused by the peeling off of the particles from the surface of the wear traces are observed. A large number of peeling pits are distributed on the surface, which is a characteristic of fatigue wear [33]. Accordingly, the wear of the TiB₂ thin film is mainly due to fatigue and abrasion.

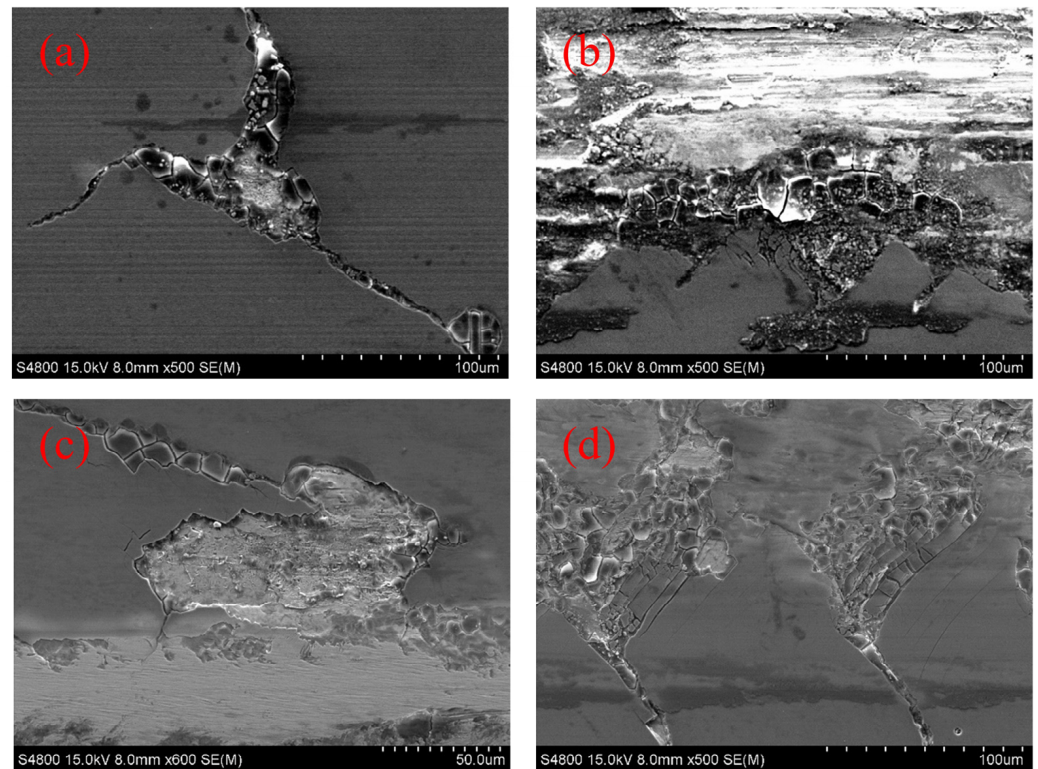


Figure 16. SEM images of the abrasion marks of the TiB₂ thin film at (a) 2 Hz, 500 \times ; (b) 4 Hz, 500 \times ; (c) 6 Hz, 600 \times ; and (d) 8 Hz, 500 \times .

4. Conclusions

In this study, a hard TiB₂ thin film possessing a uniform and dense structure was prepared at a low temperature using HiPIMS. And the film has preferred (001) and (101) crystal phases. The tribological properties of the deposited film at different friction loads and sliding frequencies were studied. The results indicate that the TiB₂ thin film possesses satisfactory tribological properties with a low friction coefficient of 0.6 and a low wear rate of $3.66 \times 10^{-6} \text{ mm}^3/(\text{N}\cdot\text{m})$ under a friction load of 5 N. Under high loads, the tribological performance of the TiB₂ thin film was poor. The wear rates are small and do not differ significantly at different sliding frequencies, reaching a small coefficient of $10^{-6} \text{ mm}^3/(\text{N}\cdot\text{m})$ level. Based on the morphology and composition analyses of the wear marks, the wear of the TiB₂ thin film was mainly dominated by fatigue wear and abrasive wear.

Author Contributions: Conceptualization, P.Z.; methodology, P.Z. and V.L.; validation, P.Z. and J.Y.; formal analysis, P.Z. and J.Y.; investigation, J.Y.; resources, P.Z., P.Y. and J.Y.; data curation, P.Z. and J.Y.; writing—original draft preparation, J.Y.; writing—review and editing, P.Z., P.Y., C.L. (Changhong Lin), T.Y., J.W., C.L. (Chen Li) and M.H.; visualization, J.Y.; supervision, P.Z., J.W., M.H. and V.L.; project administration, P.Z.; funding acquisition, V.L. All authors have read and agreed to the published version of the manuscript.

Funding: This work was financially supported by the Zhejiang Provincial Natural Science Foundation of China (No. LQ22E010007 and No. LTZ20E020001), Wenling Key Research and Development Project (No. 2023G00007), and Taizhou Science and Technology Plan Project (No. 22gya09).

Institutional Review Board Statement: Not applicable.

Informed Consent Statement: Not applicable.

Data Availability Statement: All data are available in this paper.

Conflicts of Interest: The authors declare no conflicts of interest.

References

1. Akhtar, S.S. A critical review on self-lubricating ceramic-composite cutting tools. *Ceram. Int.* **2021**, *47*, 20745–20767. [CrossRef]
2. Liu, X.; Wang, Y.; Qin, L.; Guo, Z.; Lu, Z.; Zhao, X.; Dong, H.; Xiao, Q. Friction and wear properties of a novel interface of ordered microporous Ni-based coating combined with MoS₂ under complex working conditions. *Tribol. Int.* **2023**, *189*, 108970. [CrossRef]
3. Kumar, A.; Kumar, M.; Taylor, S. Self-lubricating composite coatings: A review of deposition techniques and material advancement. In *Materials Today: Proceedings*; Elsevier: Amsterdam, The Netherlands, 2023. [CrossRef]
4. Yan, Z.; Liu, J.; Zhang, X.; Hao, J.; Liu, W. WS₂-Ti-based solid-liquid synergetic lubricating coating with super-high wear resistance for space application. *Surf. Coat. Technol.* **2024**, *476*, 130245. [CrossRef]
5. Zhao-yun, Z.; Ze-wen, D.; Hai-xia, J.; Bei-bei, Z.; Xiao-yu, Z.; You-zhi, W.; Peng, W. The Influence of Doped Ti Element on Structure and Tribological Properties of WS₂ Film. *Surf. Technol.* **2022**, *51*, 239–247+266.
6. Mingling, X.; Guang'an, Z.; Xing, S.; Xi, T.; Xiaoping, G.; Yuzhe, S. Anti-oxidization and Electronic Properties of Ti Doped MoS₂ Films. *Chin. J. Mater. Res.* **2021**, *35*, 59–64.
7. Deepthi, B.; Barshilia, H.C.; Rajam, K.S.; Konchady, M.S.; Kvit, A.V. Structure, morphology and chemical composition of sputter deposited nanostructured Cr-WS₂ solid lubricant coatings. *Surf. Coat. Technol.* **2010**, *205*, 565–574. [CrossRef]
8. Cui, S.; Li, W.-S.; He, L.; Feng, L.; An, G.-S.; Hu, W.; Hu, C.-X. Tribological behavior of a Ni-WS₂ composite coating across wide temperature ranges. *Rare Met.* **2019**, *38*, 1078–1085. [CrossRef]
9. Li, P.; Xu, F.; Robertson, S.; Zhou, Z.; Hou, X.; Clare, A.T.; Aboulkhair, N.T. Metallurgical reactions and tribological properties of self-lubricating Al-WS₂ composites: Laser powder bed fusion Vs. spark plasma sintering. *Mater. Des.* **2022**, *216*, 110543. [CrossRef]
10. Li, S.; Deng, J.; Yan, G.; Zhang, K.; Zhang, G. Microstructure, mechanical properties and tribological performance of TiSiN-WS₂ hard-lubricant coatings. *Appl. Surf. Sci.* **2014**, *309*, 209–217. [CrossRef]
11. Bibeye Jahaziel, R.; Krishnaraj, V.; Sudhagar, S.; Geetha Priyadarshini, B. Improving dry machining performance of surface modified cutting tools through combined effect of texture and TiN-WS₂ coating. *J. Manuf. Process.* **2023**, *85*, 101–108. [CrossRef]
12. Serra, E.C.; Soares, V.F.D.; Fernandez, D.A.R.; Hübler, R.; Juste, K.R.C.; Lima, C.L.; Tentardini, E.K. Influence of WS₂ content on high temperature wear performance of magnetron sputtered TiN-WS_x thin films. *Ceram. Int.* **2019**, *45*, 19918–19924. [CrossRef]
13. Xie, Z.-W.; Wang, L.-P.; Wang, X.-F.; Huang, L.; Lu, Y.; Yan, J.-C. Mechanical performance and corrosion behavior of TiAlSiN/WS₂ multilayer deposited by multi-plasma immersion ion implantation and deposition and magnetron sputtering. *Trans. Nonferrous Met. Soc. China* **2011**, *21*, s470–s475. [CrossRef]
14. Sala, N.; Abad, M.D.; Sánchez-López, J.C.; Crueira, F.; Ramos-Masana, A.; Colominas, C. Influence of the carbon incorporation on the mechanical properties of TiB₂ thin films prepared by HiPIMS. *Int. J. Refract. Met. Hard Mater.* **2022**, *107*, 105884. [CrossRef]
15. Wu, Z.; Ye, R.; Bakhit, B.; Petrov, I.; Hultman, L.; Greczynski, G. Reprint of: Improving oxidation and wear resistance of TiB₂ films by nano-multilayering with Cr. *Surf. Coat. Technol.* **2022**, *442*, 128602. [CrossRef]
16. Polyakov, M.N.; Morstein, M.; Maeder, X.; Nelis, T.; Lundin, D.; Wehrs, J.; Best, J.P.; Edwards, T.E.J.; Döbeli, M.; Michler, J. Microstructure-driven strengthening of TiB₂ coatings deposited by pulsed magnetron sputtering. *Surf. Coat. Technol.* **2019**, *368*, 88–96. [CrossRef]
17. Ozkan, D.; Yilmaz, M.A.; Bakdemir, S.A.; Sulukan, E. Wear and Friction Behavior of TiB₂ Thin Film-Coated AISI 52100 Steels under the Lubricated Condition. *Tribol. Trans.* **2020**, *63*, 1008–1019. [CrossRef]
18. Jinhui, D.; Wang, P.; Yin, L.; Feng, H.; Xikun, Y. Microstructure and friction properties of WS₂/TiB₂ solid self-lubricant coating. *Heat Treat. Met.* **2016**, *41*, 104–109.
19. Jin-long, L.; Hong-xuan, L.; Li, J.; Xiao-hong, L.; Ding-jun, Z. Tribological Properties of TiB₂ Doped WS₂ Composite Films in Wide Temperature Range. *Surf. Technol.* **2023**, *52*, 235–245.
20. Dorri, S.; Palisaitis, J.; Greczynski, G.; Petrov, I.; Birch, J.; Hultman, L.; Bakhit, B. Oxidation kinetics of overstoichiometric TiB₂ thin films grown by DC magnetron sputtering. *Corros. Sci.* **2022**, *206*, 110493. [CrossRef]
21. Hellgren, N.; Zhirkov, I.; Sortica, M.A.; Petruhins, A.; Greczynski, G.; Hultman, L.; Rosen, J. High-power impulse magnetron sputter deposition of TiB_x thin films: Effects of pulse length and peak current density. *Vacuum* **2024**, *222*, 113070. [CrossRef]
22. Feng, A.X.; Zhang, Y.K.; Xie, H.K.; Fan, Z. Characterization of Interfacial Adhesion and Bond Strength between Thin Film Coating and Substrate by Scratch Testing. *J. Jiangsu Univ. (Nat. Sci. Ed.)* **2003**, *24*, 15–19.
23. Ge, F.; Zhu, P.; Wang, H.; Meng, F.; Li, S.; Huang, F. Friction and wear behavior of magnetron co-sputtered V-Si-N coatings. *Wear* **2014**, *315*, 17–24. [CrossRef]

24. Nedfors, N.; Primetzhofner, D.; Zhirkov, I.; Palisaitis, J.; Persson, P.O.Å.; Greene, J.E.; Petrov, I.; Rosen, J. The influence of pressure and magnetic field on the deposition of epitaxial TiB_x thin films from DC magnetron sputtering. *Vacuum* **2020**, *177*, 109355. [[CrossRef](#)]
25. Leyland, A.; Matthews, A. On the significance of the H/E ratio in wear control: A nanocomposite coating approach to optimised tribological behaviour. *Wear* **2000**, *246*, 1–11. [[CrossRef](#)]
26. Lenz, B.; Hasselbruch, H.; Großmann, H.; Mehner, A. Application of CNN networks for an automatic determination of critical loads in scratch tests on a-C:H:W coatings. *Surf. Coat. Technol.* **2020**, *393*, 125764. [[CrossRef](#)]
27. Bird, A.; Yang, L.; Wu, G.; Inkson, B.J. Failure mechanisms of diamond like carbon coatings characterised by in situ SEM scratch testing. *Wear* **2023**, *530–531*, 205034. [[CrossRef](#)]
28. Zawischa, M.; Makowski, S.; Kuczyk, M.; Weihnacht, V. Comparison of fracture properties of different amorphous carbon coatings using the scratch test and indentation failure method. *Surf. Coat. Technol.* **2022**, *435*, 128247. [[CrossRef](#)]
29. Kabir, M.S.; Zhou, Z.; Xie, Z.; Munroe, P. Scratch adhesion evaluation of diamond like carbon coatings with alternate hard and soft multilayers. *Wear* **2023**, *518–519*, 204647. [[CrossRef](#)]
30. Lin-xiu, G. Introduction to the wear loss of metal materials and protection measures. *Dev. Guide Build. Mater.* **2020**, *18*, 25–26.
31. Chi, X.; Yuan, J.; Li, J.; Pan, G.; Cui, Y.; Li, X. Effect of Cu on the high-temperature wear behavior of FeAl-TiB₂ coatings produced by extreme high-speed laser cladding. *Appl. Surf. Sci. Adv.* **2023**, *17*, 100439. [[CrossRef](#)]
32. Bao, Y.; Huang, L.; An, Q.; Zhang, R.; Geng, L.; Ma, X.; Tang, G.; Zhang, H. Wear resistance of TiB/Ti composite coating fabricated by TIG cladding using Ti-TiB₂ cored wire. *Surf. Coat. Technol.* **2023**, *474*, 130086. [[CrossRef](#)]
33. Chen, L.; Zhang, X.; Zheng, W.; Wang, M.; Liu, B.; Sun, W. Investigation on corrosion behaviors and mechanical properties of TiB₂/7075Al composites with various particle contents. *J. Mater. Res. Technol.* **2023**, *23*, 2911–2923. [[CrossRef](#)]

Disclaimer/Publisher’s Note: The statements, opinions and data contained in all publications are solely those of the individual author(s) and contributor(s) and not of MDPI and/or the editor(s). MDPI and/or the editor(s) disclaim responsibility for any injury to people or property resulting from any ideas, methods, instructions or products referred to in the content.